This is the peer reviewed author accepted manuscript (post print) version of a published work that appeared in final form in:

Yu, Qi, Li, Xuegang, Zhou, Xue, Gao, Xinjei, Lv, Riqing, Nguyen, Linh V, Warren-Smith, Stephen C, Zhao, Yong 2022 'Temperature compensated fiber optic magnetic sensor based on the combination interference principle', Optics Letters, vol. 47, no. 10, pp. 2558-2561

This un-copyedited output may not exactly replicate the final published authoritative version for which the publisher owns copyright. It is not the copy of record. This output may be used for non-commercial purposes.

The final definitive published version (version of record) is available at:
https://doi.org/10.1364/OL.456552

Persistent link to the UniSA Research Outputs Repository:
https://researchoutputs.unisa.edu.au/11541.2/29540

General Rights

Copyright and moral rights for the publications made accessible in the UniSA Research Outputs Repository are retained by the authors and/or other copyright owners and it is a condition of accessing publications that users recognize and abide by the legal requirements associated with these rights.

- Users may download and print one copy for the purpose of private study or research.
- You may not further distribute the material or use it for any profit-making activity or commercial gain
- You may freely distribute the persistent link identifying the publication in the UniSA Research Outputs Repository

If you believe that this document breaches copyright, please contact us and provide details. We will remove access to the work immediately and investigate your claim.

Temperature compensated fiber optic magnetism sensor based on combination interference principle

QI YU[1#], XUEGANG LI[1,2#*], XUE ZHOU[1], XINJIE GAO[1], RIQING LV[1,2], LINH V. NGUYEN[3,4], STEPHEN C. WARREN-SMITH[3,4], YONG ZHAO[1,2,*]

[1]*College of Information Science and Engineering, Northeastern University, Shenyang 110819, China*
[2]*Hebei Key Laboratory of Micro-Nano Precision Optical Sensing and Measurement Technology*
[3]*Future Industries Institute, University of South Australia, Mawson Lakes, SA 5095, Australia*
[4]*Institute for Photonics and Advanced Sensing, School of Physical Sciences, The University of Adelaide, Adelaide, SA 5005, Australia*
**Corresponding author: lixuegang@ise.neu.edu.cn; zhaoyong@ise.neu.edu.cn;*

[#]*First author: QI YU and XUEGANG LI contributed equally to this work.*

Received XX Month XXXX; revised XX Month, XXXX; accepted XX Month XXXX; posted XX Month XXXX (Doc. ID XXXXX); published XX Month XXXX

In this paper, a highly sensitive temperature compensated fiber optic magnetic field sensor by Sagnac and Mach-Zehnder combination interference (SMZI) is proposed and verified. The sensing structure relies on microstructured exposed core fiber (ECF) filled with ethanol and magnetic fluid (MF). The refractive index (RI) of MF and ethanol is affected by magnetic field and temperature (MFT). SMZI is based on multimode and birefringence characteristics of ECF. The measurement principle is that the spectra of Sagnac interference (SI) and Mach-Zehnder interference (MZI) have respective sensitivities to MFT. The magnetic sensitivity can reach 1.17 nm/mT, and the temperature sensitivity is up to -1.93 nm/°C. At the same time, the sensor has good repeatability and low detection limits (LODs) of 0.41 mT and 0.25 °C. It not only solves the cross-influence of temperature but makes the spectral analysis more intuitive. The sensor has a broad development prospect in the application of MFT detection. © 2020 Optica Publishing Group

Fiber optic interferometers have attracted considerable attention in the sensing field because of their advantages of small size, simple fabrication and high measurement accuracy [1-4]. They can be implemented based on Mach-Zehnder [5], Michelson [6], Fabry–Perot (FP) [7] and Sagnac interference (SI) [8] effects. Each interferometer has specific advantages and responses to specified physical quantities. Therefore, magnetic fluid (MF) has been widely combined with fiber optic interferometer to form various excellent magnetic field sensors due to its good fluidity and refractive index (RI) controllability. For example, in 2013, Wang *et al.* applied MF to Mach-Zehnder interference (MZI) and obtained a sensitivity of −0.17 nm/mT [9]. Shi *et al.* used the magnetostrictive effect of MF combined with FP interferometer to measure magnetic field [10]. Deng *et al.* designed fiber optic magnetic field sensors by integrating Michelson interferometer and MF [11]. These sensors have compact structures and high integration, but they do not take into account the influence of temperature on the spectral shift in measurement, resulting in inaccurate experimental results. To reduce the measurement errors, many scholars consider that fiber optic magnetic sensors based on MF need temperature compensation. In 2018, we demonstrated that inject the MF into the photonic crystal fiber to obtain magnetic field and temperature (MFT) sensitivity of 0.72 nm/mT and -0.08 nm/°C, correspondingly [12]. Qin *et al.* recently designed a sensor with the sensitivities of 0.97 nm/mT and 0.92 nm/°C with the help of optical couplers and MF [13]. However, these dual-parameter sensors have low sensitivities and only use one interference principle to analyze two variables, resulting in a more complex demodulation spectrum and a small dynamic range. Therefore, for working out the above issues existing in the previous sensors, a combination interferometer is proposed in this paper to achieve MFT measurement.

In this paper we demonstrate a Sagnac and Mach-Zehnder combination interference (SMZI) based on exposed core fiber (ECF) for the measurement of MFT. We propose the sensor structure in combination with the characteristics of simple fabrication, easy generation of MZI, and high sensitivity of SI to RI changes. The ECF has birefringence characteristics due to its asymmetric structure, and its electron microscopic view of a cross section is shown in the illustration of Fig. 1. Thus, ECF can be used as a birefringent fiber. At the same time, ECF is also a multimode fiber due to its high numerical aperture, so the higher order modes excited at the fusion point of ECF and single-mode fiber (SMF) will lead to the multimode MZI in the core of ECF. Therefore, the system can generate SI and MZI simultaneously.

We filled the ECF's two closed air holes with ethanol and injected MF into the exposed side to magnify the birefringence value. The schematic diagram of the proposed sensor is shown in Fig. 1. SI is formed by connecting the fabricated structure to the coupler. It also enables the sensing structure to achieve a higher temperature and magnetic field sensitivity. Because SI and MZI have distinctive sensitivities to MFT, the simultaneous detection of the two parameters can be achieved via a sensitivity matrix.

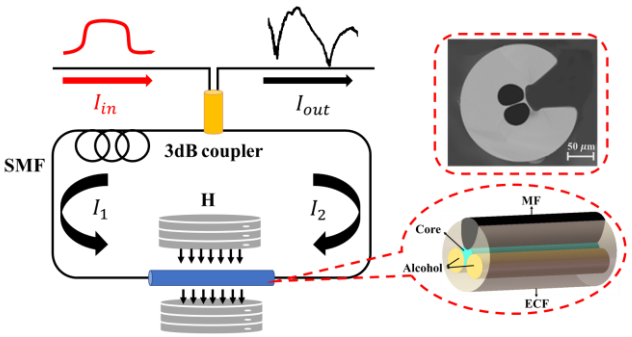


Fig. 1. Schematic diagram of Sagnac loop insertion filling ECF scheme with magnetic field (inset: electron microscopic view of ECF cross section; all air holes and exposed side of the ECF are filled with ethanol and MF).

To analyze the sensor principle, assuming that only one higher-order mode is excited at SMF/ECF, the transmitted light intensity of SI and MZI can be expressed as

$$I_{out}^{SI} = I_x + I_y + 2\sqrt{I_x I_y}\cos\left(\frac{4\pi BL}{\lambda}\right) \quad (1)$$

$$I_{out}^{MZI} = I_1 + I_2 + 2\sqrt{I_1 I_2}\cos\left(\frac{2\pi\Delta n_{eff} L}{\lambda}\right) \quad (2)$$

Where I_x and I_y represent the intensity of x and y polarization fundamental modes in ECF respectively. I_1 and I_2 are the intensity of the two beams of multimode interference. L is the length of the birefringent fiber, and B is the birefringence value. Δn_{eff} is the phase difference between I_1 and I_2. λ is the operating wavelength. The relations of SI and MZI spectrum's free spectral range (FSR) are as follows.

$$FSR_{SI} = \frac{\lambda^2}{BL} \quad (3)$$

$$FSR_{MZI} = \frac{\lambda^2}{\Delta n_{eff} L} \quad (4)$$

Because the birefringence value of the two polarization modes is much less than Δn_{eff}, FSR_{SI} is much larger than FSR_{MZI}. The phase difference of SI and MZI changes with B and Δn_{eff}, which in turn changes with the ambient RI. The RI of the liquid (MF and ethanol) selected to fill the ECF varies with the MFT, respectively. Therefore, the transmission spectrum of this structure is the function of SMZI.

The experimental system is shown in Fig. 2. The system is composed of supercontinuum light source (1200-1700 nm, Wuhan Anyang), optical spectrum analyzer (OSA, YokogawaAQ6370D) with the 0.02 nm sampling resolution, 3 dB coupler, and the proposed sensing structure. In particular, a DC power supply, a magnetic coil, and a Gauss meter (the resolution is 0.01 mT) were applied to monitor the magnetic field. The sensing structure was fabricated with ECF, MF (EMG507 concentration 2% Vol.), and anhydrous ethanol. First, the MF and ultra-pure water were diluted at a ratio of 1:1 to reduce the RI of MF, high concentration of the original MF would lead to excessive noise and no obvious interference phenomenon. Then one end of the ECF (20 cm) was immersed in ethanol, and the air holes of the entire ECF were filled with ethanol through capillary action. The ECF was fused with SMF at both ends by an optical fiber splicer (S184NM-SLDF). The exposed side was then filled with MF. Finally, the fabricated probe was placed in a capillary tube and encapsulated using UV glue.

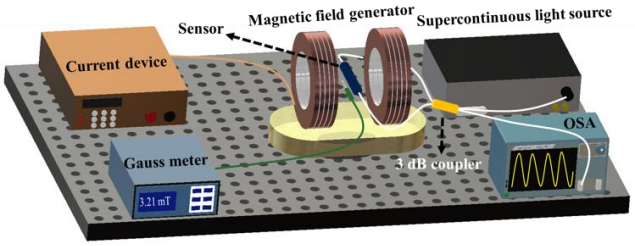


Fig. 2. Diagram of experimental device.

In Fig. 3, we first compared the spectra of the same sensor at three stages in the fabrication process, which are the unfilled ECF, the both air holes only filled with ethanol, and the ECF filled with MF and ethanol. It is found that the shapes of FSR, loss, and interference spectrum are different among the three. Firstly, due to the birefringence of ECF, they all have obvious Sagnac dips. However, due to the small birefringence value of ECF, the FSR of SI is large and there is only one dip in the wavelength range of 1525 nm to 1610 nm. In the three spectra, the small interference fringes are produced by MZI. Because the RI difference of the MZI is much larger than SI, the FSR of MZI is much less than SI. In addition, because ECF is a multi-mode fiber, MZI is not uniform. ECF without any filling has regular MZI, while the MZI spectra of the other two become chaotic due to the multiple modes excited by the filling fluid. Meanwhile, as the ECF is progressively filled with ethanol and MF, the optical loss of the ECF increases.

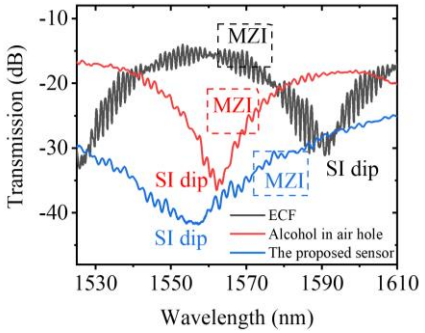


Fig. 3. Combination transmission spectra of the unfilled ECF, ethanol -filled ECF, and the ethanol and MF -filled ECF.

Fig. 4(a) shows the interference spectrum with the range of 1200 to 1680 nm without magnetic field at 23 °C (temperature near the sensor in the experiment obtained with a 1 °C resolution

thermometer). It can be observed that there are two Sagnac dips at 1250 nm and 1500 nm. In the illustration of Fig. 4(a), we amplified the spectrum in the red-shaded rectangle in Fig. 4(a) to obtain a clear MZI spectrum. It can be shown that MZI and SI occurred simultaneously in the experiment. To facilitate the analysis of the experimental results, a spectrum near 1500 nm is selected for the following bivariate detection, as shown in Fig. 4(b). For analyzing the components of the superimposed spectrum clearly, we use the Fast Fourier Transform (FFT) to demodulate the transmission spectrum in the range of 1525 to 1610 nm. The results are shown in Fig. 4(c). As expected, it can be found that the spectrum has two peaks at 0.02 nm^{-1} and 0.07 nm^{-1} as shown in the illustration. Therefore, SI and MZI spectra were obtained by filtering analysis at 0.02 nm^{-1} and 0.07 nm^{-1} respectively as shown in Fig. 4(d).

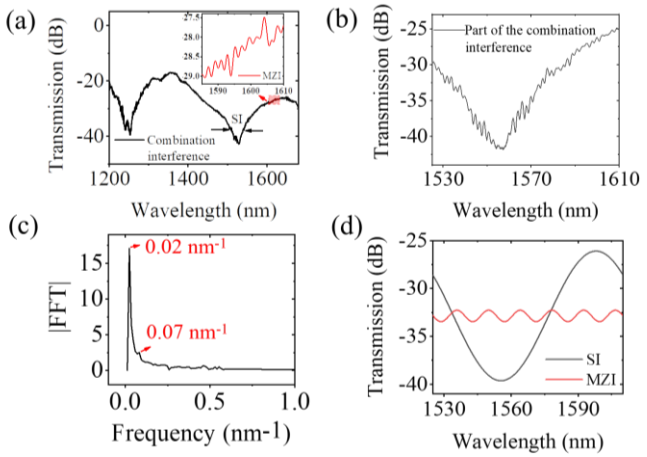


Fig. 4. (a) Combination interference spectrum (inset: MZ interference spectrum in the red shaded) (b) Intercepted spectra near the 1550 nm-Sagnac dip (c) FFT analysis in Fig.4 (b) (d) SI and MZI spectra after FFT demodulation.

Firstly, the magnetic field test was carried out. As the magnetic field strength increases, the transmission spectrum shifts. Fig. 5(a) and Fig. 5(c) correspond to the spectra of SI and MZI under different magnetic fields respectively, and it can be found that both are red-shifted with the increase of magnetic fields. The magnetic field sensitivities of SI and MZI are 1.17 nm/mT and 0.26 nm/mT. As expected, the two interferences show different sensitivities to change in the magnetic field and SI is slightly more sensitive. This is also the basis of realizing dual parameter measurement.

Next, the temperature sensing experiment without magnetic field interference was performed. The sensor structure was fixed in the middle of the thermostat (the resolution is 0.01 °C), and a thermometer probe was placed near the structure to read the temperature accurately. We measured 7 sets of data from 29 °C to 35 °C with a step size of 1 °C. Similar to the magnetic field experiment, when the temperature changes, the transmission spectrum changes. As shown in Fig. 6 (a), the SI spectrum moves significantly to the shorter wavelengths when the temperature increases. In Fig. 6(b), the dip shift corresponding to each temperature is fitted with the corresponding temperature, and it is found that they have a good linear relationship. The corresponding slope is that the temperature sensitivity of SI is -1.93 nm/°C. Similarly, the transmission spectra and corresponding sensitivity of MZI are given in Fig. 6 (c) and (d). When the temperature rises, the MZI spectrum takes on linear-like movement and the sensitivity is 0.53 nm/°C.

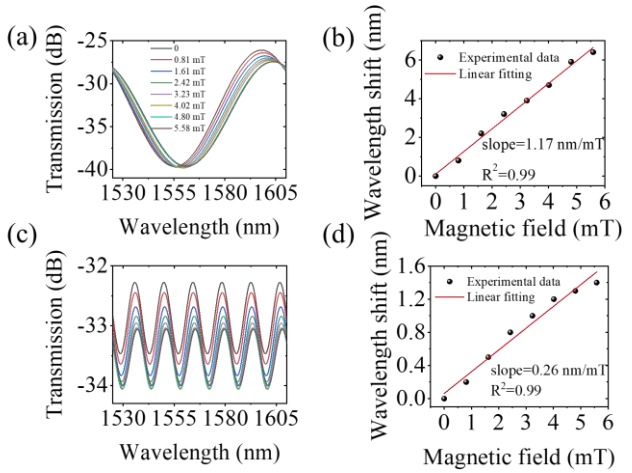


Fig. 5. (a) Filtered SI spectrum (b) SI sensitivity (c) Filtered MZI spectrum (d) MZI sensitivity under different magnetic field strength.

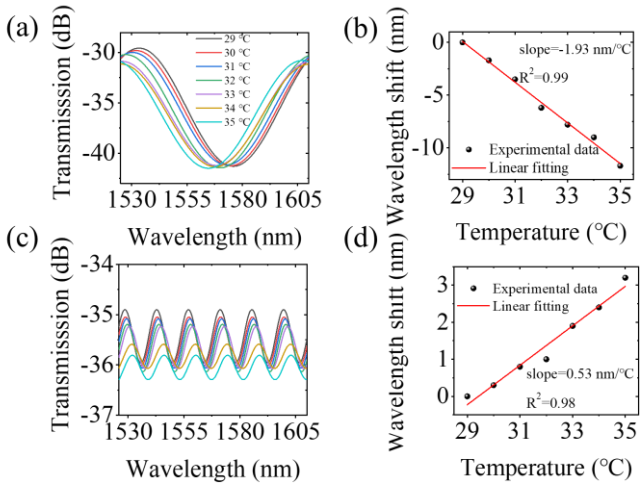


Fig. 6. (a) Filtered SI spectrum (b) SI sensitivity (c) Filtered MZI spectrum (d) MZI sensitivity under different temperatures.

The above experimental results prove that SI and MZI have different sensitivities for a single variable to be measured. The relationship between the wavelength changes and the two variables are expressed as Eq. 5

$$\begin{bmatrix} \Delta B \\ \Delta T \end{bmatrix} = \begin{bmatrix} S_{B,SI} & S_{T,SI} \\ S_{B,MZI} & S_{T,MZI} \end{bmatrix}^{-1} \begin{bmatrix} \Delta\lambda_{SI} \\ \Delta\lambda_{MZI} \end{bmatrix} \quad (5)$$

Where ΔB and ΔT represent changes in MFT, $S_{B,SI}$ and $S_{B,MZI}$ represent the magnetic field sensitivities of SI and MZI, $S_{T,SI}$ and $S_{T,MZI}$ are the SI and MZI's temperature sensitivities of the sensor. $\Delta\lambda_{SI}$ and $\Delta\lambda_{MZI}$ are the wavelength shift corresponding to SI and MZI. By substituting the corresponding values of each sensitivity, the calculation method of ΔB and ΔT can be obtained.

$$\begin{bmatrix}\Delta B\\ \Delta T\end{bmatrix}=\begin{bmatrix}1.17 & -1.93\\ 0.26 & 0.53\end{bmatrix}^{-1}\begin{bmatrix}\Delta\lambda_{SI}\\ \Delta\lambda_{MZI}\end{bmatrix} \quad (6)$$

Therefore, by observing the spectral wavelength drift of SI and MZI, the simultaneous measurement of MFT can be achieved by substituting it into Eq. 6. By calculating, the condition number of the above matrix can be obtained as 4.64. The non-singular matrix with a large condition number is called ill-conditioned matrix, whose coefficient matrix is sensitive to small perturbations, resulting in great difficulty in the numerical solution. The condition number of this matrix is not very large, so it is a non-ill-conditioned matrix and easier to compute.

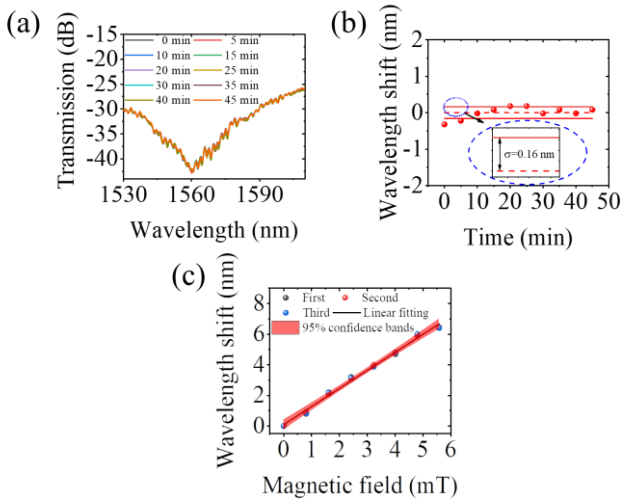


Fig. 7. (a) Spectral stability at room temperature and the same magnetic field strength (b) SI standard deviation (c) Stability experiment.

To verify the stability of the sensor, an experiment was performed at 23 °C and 5.58 mT. The spectrum was recorded every 5 mins a total of ten times. As shown in Fig. 7(a), spectra obtained at different times almost overlap. To further analyze the stability performance, we introduce the definition of low detection limit (*LOD*). *LOD* is one of the important indicators of the sensor, which can be expressed as

$$LOD = 3\sigma / S \quad (7)$$

σ is the standard deviation, S represents the sensitivity of the sensor. Bring in the maximum sensitivity of 1.17 nm/mT and -1.93 nm/°C to get the lowest *LOD*. Fig. 7(b) shows a standard deviation of 0.16 nm for spectra from different times. By calculation, the minimum *LOD* of the sensor is 0.41 mT and 0.25 °C. Then we carried out a repeatability test and repeated the experiment for three times on the sensor, as shown in Fig. 7(c). All experimental data were within the 95% confidence interval of the red band in the Fig.7(c).

Table 1 compares the sensing structure, interference principle, and sensitivity of several typical MFT dual-parameter sensors. We found that our sensor is simple to make and significantly improved sensitivity.

Based on the different sensitivities of SI and MZI to the two variables, a SMZI MFT fiber optic sensor is proposed, which fully combines the advantages of the combined interference principle, MF and ECF. Simple welding and filling techniques were chosen in the manufacturing process of the sensor. The obvious difference between MZ and SI spectra was used to make the processing process more intuitive. The proposed sensor has ultra-high sensitivity of 1.17 nm/mT and -1.93 nm/°C, good stability and repeatability. It is a low-cost, large dynamic range detection, considering the influence of temperature fiber magnetic field sensor.

Table 1. Comparison of optical fiber sensors based on different interference principles.

Sensor structure	Principle	Sensitivity (nm/mT)	Sensitivity (nm/°C)	Ref.
D-shaped fiber and coreless fiber	MZI	0.99	0.08	[14]
FBG in the FP cavity	FPI	0.53	-0.09	[15]
FBG in PCF	MZI	0.92	0.16	[16]
Two special optical fibers in Sagnac loop	SI and MZI	0.71	0.30	[17]
ECF in Sagnac loop	SI and MZI	1.17	-1.93	Our work

Funding. National Natural Science Foundation of China (61903073); Central University Basic Research Fund of China (N2204013); Australian Research Council (ARC) Future Fellowship (FT200100154); Natural Science Foundation of Hebei Province (No. F2020501040).

Disclosures. The authors declare no conflicts of interest.

Data availability. Data underlying the results presented in this paper are not publicly available at this time but may be obtained from the authors upon reasonable request.

References

1. Q. Liu, S.-M. Li, D.-P. Zhou, Z. Jing, and W. Peng, Opt. Lett. **46**, 4944-4947 (2021).
2. J. Villatoro, Opt. Lett. **45**, 21-24 (2020).
3. L. V. Nguyen, S. C. Warren-Smith, H. Ebendorff-Heidepriem, and T. M. Monro, Opt. Express **24**, 8967-8977 (2016).
4. X. Lei, X. Dong, T. Sun, and K. Grattan, Journal of Lightwave Technology **39**, 5625-5633 (2021).
5. Z. Lin, R. Lv, Y. Zhao, H. Zheng, and X. Wang, Opt Lett **46**, 2714-2717 (2021).
6. M. Deng, T. Zhang, X. Nan, Y. Tang, D. Feng, N. Guo, S. Deng, and T. Zhu, Opt. Lett. **46**, 6079-6082 (2021).
7. Y. Zhao, N. Song, F. Gao, X. Xu, J. Liu, and C. Liu, Opt. Express **29**, 32453-32463 (2021).
8. Q. Liu, L. Xing, Z. Wu, Y. Fu, S. Li, P. Xue, W. P. Ng, Q. Wu, and R. Binns, IEEE Transactions on Instrumentation and Measurement **70**, 1-9 (2021).
9. H. Wang, S. Pu, N. Wang, S. Dong, and J. Huang, Opt Lett **38**, 3765-3768 (2013).
10. F. Shi, Y. Luo, J. Che, Z. Ren, and B. J. O. F. T. Peng, **43**, 35-40 (2018).
11. M. Deng, X. Sun, M. Han, and D. J. A. O. Li, **52**, 734 (2013).
12. X. G. Li, X. Zhou, Y. Zhao, and R. Q. J. O. F. T. Lv, **41**, 1-6 (2018).
13. S. Qin, J. Lu, Y. Yu, M. Li, J. Yang, Z. Zhang, Y. Lu, and Z. Meng, Opt Express **29**, 29492-29504 (2021).
14. D. Yue, B. Wu, M. Wang, X. Han, S. Xiao, C. Sun, H. Li, S. J. O. Jian, and L. Technology, **107**, 169-173 (2018).
15. J. Xia, F. Wang, L. Hong, Q. Wang, and S. J. S. Xiong, **16**, 620 (2016).
16. J. Wang, L. Pei, J. Wang, Z. Ruan, and T. J. O. e. Ning, **28**, 1456-1471.
17. C. Sun, M. Wang, Y. Dong, S. Ye, and S. Jian, Optical Fiber Technology **48**, 45-49 (2019).